JOURNAL OF MATERIALS SCIENCE: MATERIALS IN MEDICINE 5 (1994) 516–521

Processing behaviour of hydroxyapatite powders with contrasting morphology

S. BEST, W. BONFIELD
IRC in Biomedical Materials, Queen Mary and Westfield College, Mile End Road, London E1 4NS, UK

Three synthetic hydroxyapatite powders (designated A, B and C), supplied by British Charcoals and MacDonalds and Merck GmbH were chemically and physically characterized with X-ray diffraction (XRD), infrared spectroscopy (IRS), gravimetric analysis (GA), inductively coupled plasma spectroscopy (ICPS), surface area analysis (BET), particle size analysis and scanning electron microscopy (SEM). The powders were pressed at 80 MPa and fired at a range of sintering temperatures between 1190 °C and 1300 °C for 12 h. The sintering characteristics of the four powders were assessed by density measurement, hardness testing and scanning electron microscopy. Infrared spectroscopy and X-ray diffraction results indicated that the powders showed no evidence of decomposition into tricalcium phosphate after sintering at any of the temperatures tested. However, the marked differences in morphology between the three powders led to contrasting sintering characteristics. While two of the powders sintered to near full density, the other showed very little change in density over that of the green compact even after sintering at 1300 °C. Measurement of the hardness versus sintering temperature indicated that the mechanical properties of only the two samples which sintered to full density would make them suitable for any load-bearing applications.

1. Introduction

Dense, sintered hydroxyapatite has many potential applications as a biomaterial in skeletal reconstruction. However, over recent years various publications concerning the production and sintering of hydroxyapatite ceramics have reported a wide variation in the sintering behaviour and the resultant mechanical properties [1–10]. Closer inspection of this work indicates that the hydroxyapatite powders had nominally similar chemical characteristics, but there was little information reported concerning the physical properties of the powder. There is also an absence of documentation of the comparison of the processing behaviour of morphologically distinct hydroxyapatite powders which is surprising given the very strong dependence reported of the sintering properties (and therefore mechanical properties) of ceramics in general on the morphology of the precursor powder [11–17].

Hence it is particularly important that hydroxyapatite powders should be fully characterized and any results reported should include details of morphology (including particle size distribution) and surface area, if the mechanical behaviour of hydoxyapatite powders from different sources is to be compared. This study (which is part of a larger programme concerned with the processing behaviour of hydroxyapatite) investigates the sintering behaviour of three hydroxyapatite powders of different morphologies.

2. Methods

2.1. Powder characterization

Three synthetic hydroxyapatite powders were supplied by British Charcoals and MacDonalds (designated powders A and B) and Merck GmbH (powder C). The materials were chemically and physically characterized using X-ray diffraction (XRD), infrared spectroscopy (IRS), gravimetric analysis (GA), inductively coupled plasma spectroscopy (ICPS), surface area analysis (BET), particle size analysis and scanning electron microscopy (SEM).

X-ray diffraction was performed on powder compacts with a Siemens D500 Diffractometer (attached to a PDP-micro 11/23 plus computer) using CuK_α radiation at 30 mA, 40 kV. Scans were performed between 2θ values of 0° to 65° at a rate of 0.5° min^{-1} since the strongest reflections for both hydroxyapatite and tricalcium phosphate occur within this range. Lattice parameters were calculated from the Siemens Diffrac-11 software facility modified by Dr S. Tarling, Birkbeck College, University of London. Powders were analysed in their as-received condition and after heat treatment at 1280 °C for 12 h (to simulate their condition post-sintering). The peaks were matched with the ASTM standard for hydroxyapatite and any extraneous peaks were identified using the ASTM and JCPDS standards. Full width half maximum calculations were performed on the principal peaks (in the 2θ range 31–34°) utilizing the 'Appleton' peak fitting procedure in the Siemens software package.

Infrared spectroscopy was performed using a Nicolet 730sx FTIR instrument operating in the absorbance mode. Samples were analysed in the as-received condition and after heat treatment at 1280 °C for 12 h.

0957–4530

The calcium to phosphorus ratios for the three powders was measured using gravimetric analysis as specified by British Charcoals and MacDonalds. The result was obtained by calculating the ratio of the percentage yield of CaO and P_2O_5 from precipitation reactions to produce magnesium pyrophosphate and calcium oxalate.

Inductively coupled plasma spectroscopy was performed with a Philips PV8490 I.C.P. source unit with a low pressure argon supply coupled to a Philips PV8060 spectrometer unit. Calculations were made using a DECmicro PDP 11/53 computer with Philips ES 40 software. Hydroxyapatite samples were dissolved in hydrochloric acid and filtered, before being diluted and analysed. A reference calcium phosphate sample and a blank (hydrochloric acid) sample were also prepared using this method by means of standards. Atomic absorption was performed with a Philips IL S12 AAS machine and an acetylene flame using background correction.

The morphology of powders and the fracture surfaces of sintered samples were studied using a JEOL 35 JSM scanning electron microscope with an accelerating voltage of 20 KV. Powder samples were attached to adhesive aluminium tape on an aluminium stub and sintered samples were attached to aluminium stubs by a conducting carbon cement. Samples were sputter coated for approximately 3 min using a gold/palladium target.

A Micromeretics High Speed Surface Analyser was used to determine particle surface area with the BET method. The volume of nitrogen required to adsorb as a monolayer onto the surface of accurately weighted samples of hydroxyapatite was measured at 0 °C and at − 196 °C (liquid nitrogen temperature). The procedure was repeated twice to ensure the reproducibility of the results obtained.

Particle size measurements were performed with a Malvern Particle Size Analyser using the 'Mastersizer' software facility. Samples were treated in an ultrasonic bath for 1 min using 'Dispex A40' (Allied Colloids Ltd.) in order to break up any loosely bound agglomerates prior to measurement.

2.2. Specimen preparation

Beam specimens ($5 \times 5 \times 50$ mm^3) were produced from each of the powders in the as-received condition in a single action die, lubricated with a low molecular weight hydrocarbon. A pressure of 80 MPa was exerted using a Howden mechanical press. Samples were then sintered at temperatures ranging from 1190 °C to 1320 °C at a heating rate of 2.5 °C min^{-1}, a dwell of 6 h at 400 °C (to allow the burn off of organic impurities) and a dwell of 12 h at the maximum temperature, followed by a furnace cool.

2.3. Specimen testing

The density of sintered samples was measured by Archimede's principle and the average was taken of eight readings. Hardness results were obtained from a Schimadzu microhardness testing machine with a 1 kg load. The diagonals of ten pyramidal indents were measured on as-sintered specimens to give an overall average hardness value.

3. Results

3.1. Powder characterization

Fig. 1 shows the XRD traces for each of the powders in the as-received condition. In comparison, Fig. 2 shows the traces obtained for the same powders after subsequent heat treatment at 1280 °C for 12 h. The peak positions and relative peak heights for a hydroxyapatite standard (supplied by Unilever) are shown as 'differentials' of the peaks plotted along the bottom of the traces. Comparing the two sets of traces for the powders, it is evident that no extraneous phases were detected in the range of 2θ° observed either before or after heat treatment. The lattice parameters ('*a*' and '*c*') found for the three powders and their full width half maxima (FWHM) values over the four principal peaks are displayed in Table I.

The lattice parameters for the powders matched the standard values of hydroxyapatite to within a percentage error of 0.1% and there was no significant variation between values obtained for the as-received and heat-treated conditions. The full width half maximum values indicate that there was a significant narrowing

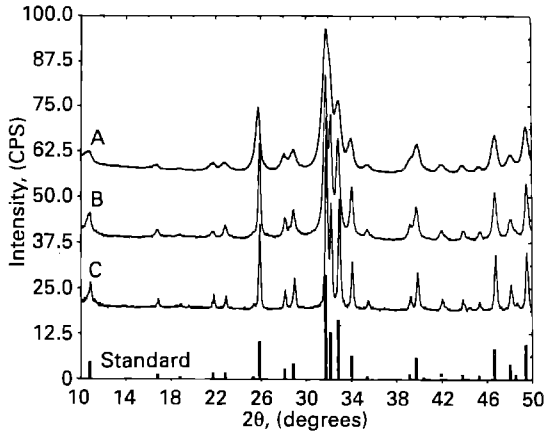

Figure 1 X-ray diffraction traces for powders A, B and C in the as-received condition.

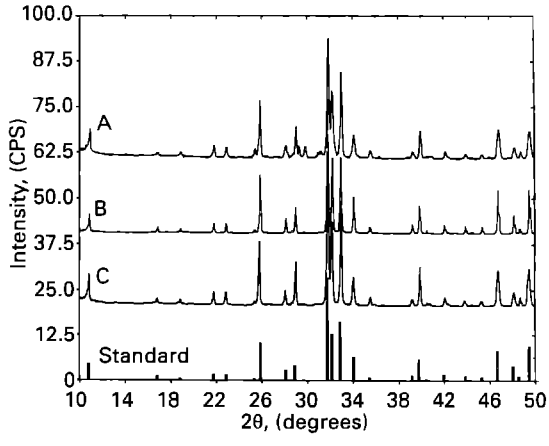

Figure 2 X-ray diffraction traces for powders A, B and C after heat treatment.

TABLE I Lattice parameters and FWHM results

Sample	As-received			Heat treated 1280 °C/12 h		
	a (nm)	*c* (nm)	FWHM	*a* (nm)	*c* (nm)	FWHM
Standard[a]	0.942	0.688	–	–	–	–
A	0.942	0.688	0.25	0.940	0.689	0.12
B	0.943	0.687	0.34	0.941	0.688	0.09
C	0.940	0.687	0.47	0.941	0.690	0.13

[a] ASTM Standard

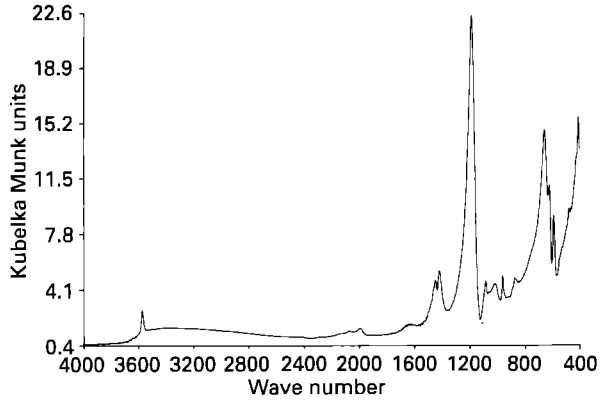

Figure 3 Typical infrared spectrum for the powders in the as-received condition.

of the peaks after heat treatment in all of the powders. Powder B had the broadest peaks in the as-received condition and showed the largest percentage change after heat treatment (73%). After heat treatment the FWHM values for the three powders were similar showing an overall percentage difference of less than 31% post-heat-treatment rather than 60% prior to heat treatment. The results indicate that either a significant amount of crystallite growth occurred or there was a large decrease in the inhomogeneous lattice strain in the powders during thermal treatment.

A typical infrared spectrum for the samples in their as-received condition is shown in Fig. 3. All of the powders showed similar traces of carbonate in their as-received condition in the form of a doublet between 1400 and 1450 cm^{-1} while the phosphate bands were poorly resolved. The water of hydration appeared as a broad band shouldered on the OH peak.

An example of a typical infrared spectrum for the samples after heat treatment at 1280 °C for 12 h is shown in Fig. 4. After heat treatment, all of the bands were sharper, indicating an increase in crystallinity. The carbonate bands disappeared in all of the samples and the phosphate bands were better resolved. However, the band associated with the water of hydration was still present.

The calcium-to-phosphorus ratios found for the three powders are shown in Table II. It can be seen that the calcium-to-phosphorus ratio found for powder C was close to the stoichiometric value for hydroxyapatite, while the values found for powders A and B indicated that they were both slightly calcium rich.

The levels of trace elements found in the three powders with ICPS and atomic absorption are shown

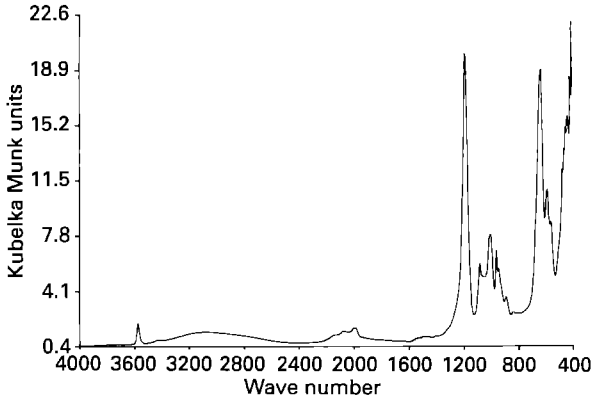

Figure 4 Typical infrared spectrum for the powders after heat treatment.

TABLE II Calcium to phosphorus ratios calculated from gravimetric analysis results

Powder	Ca : P
A	1.72(+ / − 0.015)
B	1.73(+ / − 0.01)
C	1.68(+ / − 0.003)

TABLE III ICPS and AAS results

(Wt % impurity)	A	B	C
Mn	0.02	0.02	0.03
Mg	0.31	0.30	0.48
Na	0.15	0.15	0.30
Sr	0.0003	0.0002	0.0002
Ba	0.0001	0.0001	0
Cr	< 0.0001	< 0.0001	< 0.0001
Zn	< 0.0001	0	0
Fe	0.0004	0.0007	0.0003

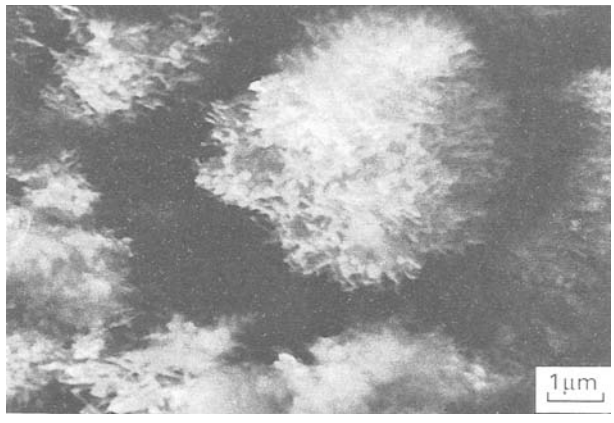

Figure 5 Scanning electron micrograph of powder A.

in Table III. Powders A and B exhibited similar concentrations of trace elements while powder C had higher magnesium and sodium levels.

Scanning electron micrographs of the three powders are shown in Figs 5–7. As illustrated in Fig. 5, the particles of powder A were irregular in shape and at higher magnifications they were seen to be composed of acicular crystallites. Powder B appeared to consist

of regular, smooth, spheroid particles which were of a larger mean diameter than those of the powder A (Fig. 6). On closer inspection, the particles could be resolved into agglomerates of crystallites of the order of 0.1 μm in size. Powder C consisted of angular fragments (up to around 100 μm in size) of a coarsely divided precipitation cake which in turn were composed of spheroid crystallites of approximately 0.5 μm in diameter (Fig. 7).

The surface areas of the powders are displayed in Table IV.

The results indicate that there was a wide variation in the surface areas of the powders with the value for the material C being over 30 times larger than that of powder B.

The particle size distribution for the three powders is shown in Fig. 8 and the values of $D_{0.1}$, $D_{0.5}$ and $D_{0.9}$ are shown in Table V.

The particle size distributions of both powder A and B were approximately monomodal. However, the mean particle size for the powder A was less than half that of powder B. Powder C showed a very broad and flat distribution which was essentially bimodal (as indicated by the large $D_{0.9}$ value).

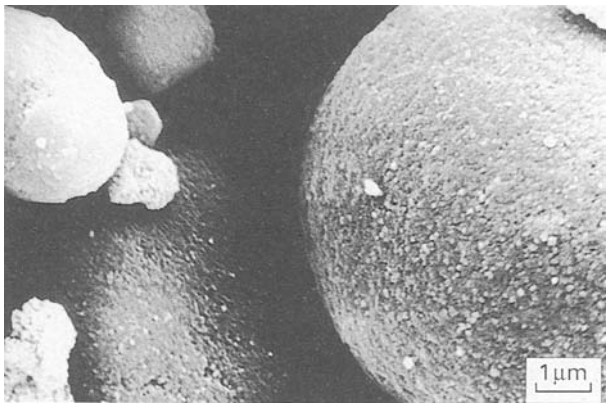

Figure 6 Scanning electron micrograph of powder B.

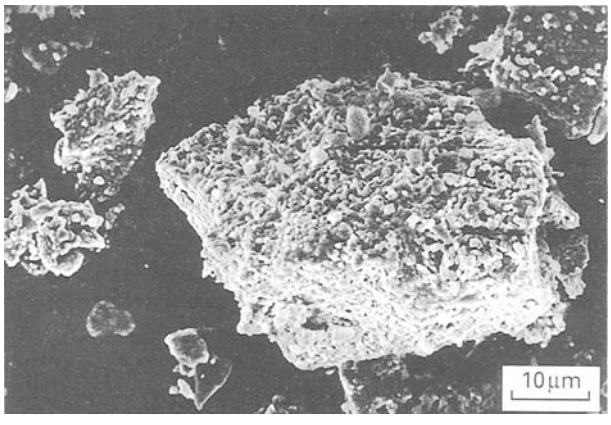

Figure 7 Scanning electron micrograph of powder C.

TABLE IV Surface area results

Powder	Surface area ($m^2\ g^{-1}$)
A	18
B	2
C	63

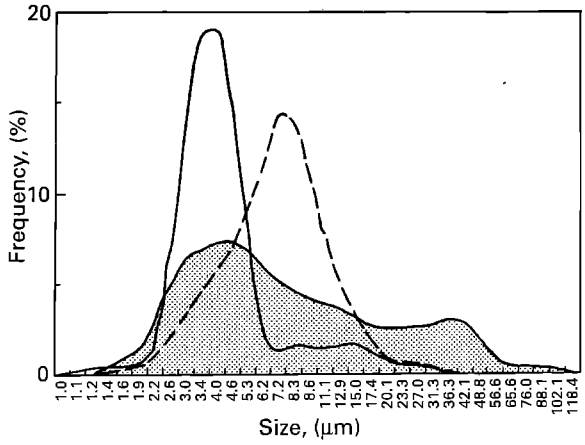

Figure 8 Particle size distribution for the powders: — A, – – – B, --- C.

TABLE V $D_{0.1}$, $D_{0.5}$ and $D_{0.9}$ values from particle size analysis

Powder	$D_{0.1}$ (μm)	$D_{0.5}$ (μm)	$D_{0.9}$ (μm)
A	2.5	3.6	7.8
B	4.2	8.7	15.4
C	4.1	20.9	54.4

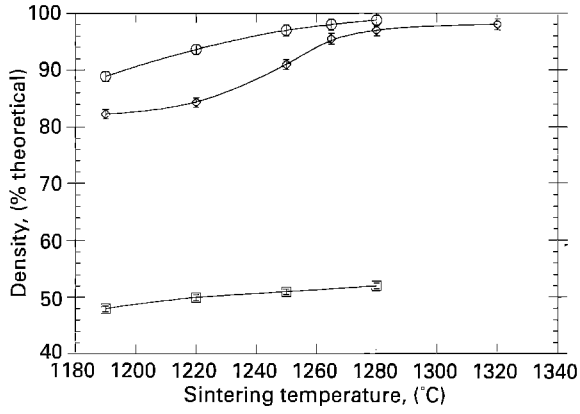

Figure 9 Variation in density with sintering temperature: □ A; ◇ B; ○ C.

3.2. Specimen testing

The variation in density with sintering temperature for the three powder is shown in Fig. 9. While powders A and C showed an expected increase in density with increasing sintering temperature, powder B showed a limited increase in density over that of the green compact, even after sintering at 1300 °C for 12 h. Powders C and A reached maximum densities of 98.8% and 97%, respectively, of the theoretical density for hydroxyapatite (3.156 $Mg\,m^{-3}$), respectively, after sintering at 1280 °C.

The variation of hardness with sintering temperature for the three materials is shown in Fig. 10. Again it is evident that while materials A and C showed a

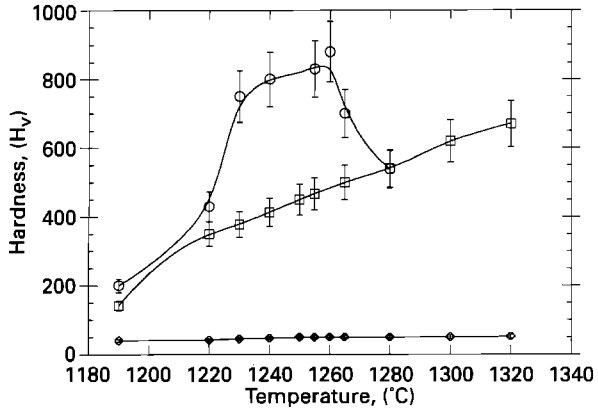

Figure 10 Variation in hardness with sintering temperature: □ A; ◇ B; ○ C.

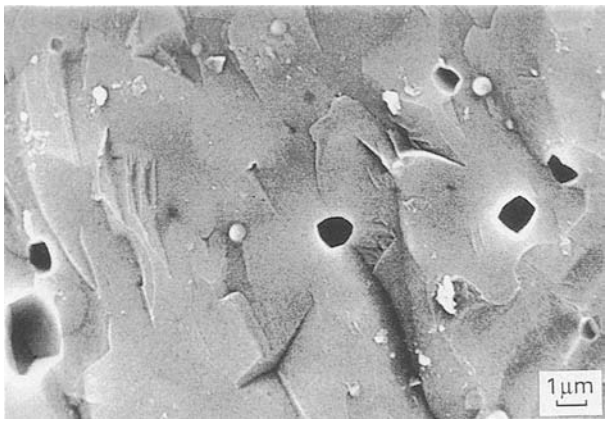

Figure 11 Scanning electron micrograph of the fracture surface of material A after sintering at 1280 °C.

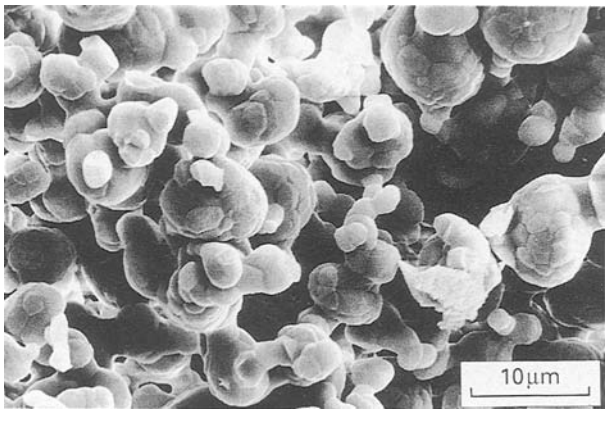

Figure 12 Scanning electron micrograph of the fracture surface of material B after sintering at 1280 °C.

marked increase in hardness with sintering temperature, the hardness of material B remained of the order of 50 H_V, even after sintering at 1300 °C for 12 h. Material C showed a much more rapid increase in hardness with sintering temperature, peaking at 880 H_V after sintering at 1265 °C while material A showed a peak hardness of 680 H_V after sintering at 1280 °C.

Figs 11–13 show the fracture surfaces of the three materials after sintering at 1280 °C for 12 h. Materials

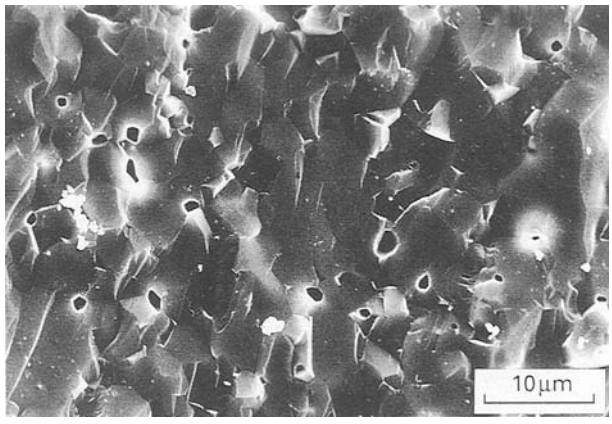

Figure 13 Scanning electron micrograph of the fracture of material C after sintering at 1280 °C.

A and C both exhibited intergranular fracture and show very little porosity. However, the particles of material B showed only the beginnings of neck formation after sintering at 1280 °C. Closer inspection of these particles revealed that the nanometre scale crystallites observed in the as-received powder appeared to have sintered to give an intra-particle grain structure.

4. Discussion

A number of groups have reported methods of producing and sintering hydroxyapatite [1–10], but very few document in detail the physical characteristics of their material. Normally, a particle size is quoted, but less frequently is there any mention of the surface area, particle size distribution or morphology of the powder. Nagai and Nishimura [10], Akao *et al.* [1], Kijima and Tsutsumi [7] and Jarcho *et al.* [6] all precipitated hydroxyapatite and estimated crystallite sizes using XRD and electron microscopy, but no surface area measurements were reported. A more complete material characterization was reported by Denissen *et al.* [2] who reported surface area and particle size range. Denissen *et al.* compared commercial powders with their own, laboratory-made material and found that their material was composed of 'fine' particles and had a surface area of 80–90 $m^2 g^{-1}$ as compared with the commercial powders which had particle sizes of 50–300 μm and 1–2 μm and surface areas of 45 and 59 $m^2 g^{-1}$ respectively. Rootare and Craig [8] used hydroxyapatite powder with a surface area of 70 $m^2 g^{-1}$ and a bulk density of 0.586 $g cm^{-3}$ and a median particle size of 8 μm. However, none of the groups gave information concerning particle size distribution.

Gravimetric analysis results from the powders used in this study indicated that powders A and B were slightly calcium rich, while the calcium-to-phosphorus ratio for powder C was close to the stoichiometric value. However, both X-ray diffraction and infrared analyses gave very similar results for all three powders with no extraneous phases in the XRD traces and only a small trace of carbonate in the infrared spectra.

The physical characteristics of the powders were in marked contrast. While powder C was composed of

high surface area 100 μm-scale soft agglomerates of spheroidal, submicrometre particles, the powders A and B were composed of hard agglomerates, which had been subjected to some form of pre-sintering stage. The intermediate surface area measured for powder A was due to the surface area created by the needle-shaped crystallites, which agglomerated to give the 3-μm size secondary particles their 'fluffy' appearance. However, the nanometre-scale crystallites which comprised the particles of powder B appeared to be much more tightly packed to give an almost smooth appearance to the 8–10 μm secondary particles. Referring to the X-ray diffraction traces and Table I, the full width half maximum values calculated for the materials in their as-received condition confirm the observation that the crystallite size in powder C is substantially larger than that of powder B.

A wide range in the densification characteristics and mechanical behaviour of hydroxyapatite have been reported previously ranging from densities of 97% and 92.5% with associated hardnesses of 450 H_V and 260 H_V, respectively, after sintering at 1200 °C for 6 h [2] to a density of 98.9% and a hardness of 650 H_V after sintering at 1150 °C for 1 h [7]. The very different sintering behaviour of the materials considered in this study may be explained in terms of the physical characteristics of the powder. The high surface area and small mean primary particle size of material C meant that there was a large driving force for densification. The spheroidal morphology of the primary particles also led to a green compact with good particle–particle contact. Hence material C sintered well, to high density, with the pore shape and size both uniform and regular. Powder A consisted of hard agglomerates of acicular crystallites which would have led to a lower packing density in the green state. The surface area of the powder was significantly lower than that of material C and hence there would have been a large variation in the size and shape of the spaces between the particles in the green compact. These factors would all contribute to a reduction in the overall density of a compact sintered to any given temperature as compared with powder C. Powder B might have appeared, at first sight, to have been an ideal material to be sintered to near full density: the monomodal distribution of smooth, spheroid particles should have led to a good packing density. However, the results indicated that during the heat treatment cycle, the particles themselves densified and the crystallites took on the form of grains within the particles. Continued application of heat led to grain growth with the particles and only the beginnings of neck formation could be observed between them. Hence, once the crystallites had sintered within the spheroid particles there was minimal driving force for the densification of the powder compact as a whole.

5. Conclusions

The work reported in this paper has indicated the contrasting sintering behaviour of three chemically similar, but morphologically different hydroxyapatite powders. The mechanical properties of sintered hydroxyapatite are determined not only by the powder chemical composition median particle size and processing conditions as shown previously, but also by the particle size distribution, surface area and particle particle morphology.

Acknowledgements

The authors gratefully acknowledge the provision of a CASE research studentship (S. Best) by the SERC and British Charcoals and MacDonalds. We would also like to thank the following for their experimental assistance and useful discussions: Dr S. Tarling and Mr M. Vickers (Department of Crystallography, Birkbeck College, University of London), Dr R. Smith (IRC in Biomedical Materials, Queen Mary and Westfield College, University of London), Professor K. DeGroot and Mr J. Wolke, (Department of Biomaterials, University of Leiden) and Mr M. Real.

References

1. M. AKAO, H. AOKI and K. KATO, *J. Mater. Sci.* **16** (1981) 809.
2. H. W. DENISSEN, K. DEGROOT, A. A. DRIESSEN, J. G. C. WOLKE, J. G. J. PEELEN, H. J. A. VAN DIJK, A. P. GEHRING and P. J. KLOPPER, *Sci. Ceram.* **10** (1980) 63.
3. G. DE WITH, H. J. A. VAN DIJK and N. HATTU, *Proc. Brit. Ceram. Soc.* **31** (1981) 181.
4. G. DE WITH, H. J. A. VAN DIJK, N. HATTU and K. PRIJS, *J. Mater. Sci.* **16** (1981) 1592.
5. A. A. DRIESSENS, C. P. A. T. KLEIN and K. DEGROOT, *Biomaterials (Commun.)* **3** (1982) 113.
6. M. JARCHO, C. H. BOLEN, M. B. THOMAS, J. BOBICK, J. F. KAY and R. H. DOREMUS, *J. Mater. Sci.* **11** (1976) 2027.
7. T. KIJIMA and M. TSUTSUMI, *J. Amer. Ceram. Soc.* **62** (1979) 455.
8. H. ROOTARE and R. G. CRAIG, *J. Oral Rehab.* **5** (1978) 293.
9. M. B. THOMAS, R. H. DOREMUS, M. JARCHO and R. L. SALSBURY, *J. Mater. Sci.* **15** (1980) 891.
10. H. NAGAI and Y. NISHIMURA, US Patent no. 4,548,59, October 1985.
11. E. BARRINGER, N. JUBB, B. FEGLEY, R. L. POBER and H. K. BOWEN, in "Ultrastructure processing of ceramics and glasses", edited by L. L. Hench and D. R. Ulrich (Wiley, New York, 1984) p. 315.
12. N. STEWARD, PhD Thesis, Imperial College, University of London (1989) p. 68.
13. M. F. YAN, *Mater. Sci. Eng.* **48** (1981) 53.
14. S. BEST, W. BONFIELD and C. DOYLE, in "Bioceramics 1: Proceedings of the 1st International Bioceramic Symposium", edited by H. Oonishi H. Aoki and K. Sawai (Ishiyaku Euro-America Inc., 1989) p. 68.
15. *Idem.*, in "Bioceramics 2: Proceedings of the 2nd International Symposium on Ceramics in Medicine", edited by G. Heimke (Deutsche Keramische Gesellschaft e.V, 1990) p. 57.
16. S. PUAJINDANETR, S. BEST and W. BONFIELD, in "Bioceramics 5: Proceedings of the 5th International Symposium on Ceramics in Medicine", edited by T. Yamamuro, T. Kukubo and T. Nakamura (Kobunshi Kankikai Inc., 1992) p. 23.
17. S. BEST, PhD Thesis, University of London, 1990.

Received 10 May and
accepted 20 December 1993